

# Variations in Optical Sensor Pressure Measurements due to Temperature in Wind-Tunnel Testing

Andrei Vladimir Popov\* and Ruxandra Mihaela Botez†

École de Technologie Supérieure, Montréal, Québec H3C 1K3, Canada

Mahmoud Mamou‡

National Research Council, Ottawa, Ontario K1A 0R6, Canada

and

Lucian Teodor Grigorie§

École de Technologie Supérieure, Montréal, Québec H3C 1K3, Canada

DOI: 10.2514/1.40715

In this paper, wind-tunnel measurements are presented for the airflow fluctuation detection using pressure optical sensors. Twenty-one wind-tunnel test runs for various Mach numbers, angles of attack, and Reynolds numbers were performed in the  $6 \times 9 \text{ ft}^2$  wind tunnel at the Institute for Aerospace Research at the National Research Council Canada. A rectangular finite aspect ratio half-wing, having a NACA 4415 cross section, was considered with its upper surface instrumented with pressure taps, pressure optical sensors, and one Kulite transducer. The Mach number was varied from 0.1 to 0.3 and the angle of attack range was within  $-3$  to  $3$  deg. Unsteady pressure signals were recorded and a thorough comparison, in terms of unsteady and mean pressure coefficients, was performed between the measurements from the three sets of pressure transducers. Temperature corrections were considered in the pressure measurements by optical sensors. Comparisons were also performed against theoretical predictions using the XFOIL computational fluid dynamics code, and mean errors smaller than 10% were noticed between the measured and the predicted data.

## Nomenclature

$C_p$	= pressure coefficient
$c$	= chord
$M$	= Mach number
$N$	= natural logarithm of rapport between amplified perturbation and initial perturbation in laminar flow
$N_{cr}$	= $N$ critical, the value of $N$ when transition between laminar and turbulent flow occurs
$p_{abs}$	= absolute pressure
$p_{gage}$	= gage pressure
$p_0$	= total pressure (stagnation pressure)
$p_\infty$	= inflow static pressure
$Re$	= Reynolds number
$\alpha$	= angle of attack

## I. Introduction

THE modern era of aviation opened a new horizon of research for drag reduction through morphing an adaptive wing, which is motivated by rising fuel costs and environmental concerns. The concept relies on delaying the transition location toward the wing trailing edge by morphing the upper surface of the wing. Several

authors have studied this concept from a theoretical point of view [1,2]. The main objective of this concept is to promote large laminar regions on the wing surface, thus reducing drag over an operating range of flow conditions characterized by Mach numbers, airspeeds, and angles of attack [3]. The airborne modification of an aircraft wing airfoil shape can be realized continuously to maintain laminar flow over the wing surface as flight conditions change. To achieve such a full operating concept, a closed control system has to be developed to link the flow fluctuations over the wing surface to the deformation mechanism (actuators). The flow fluctuation signals can be detected by conventional pressure transducers or the new emerging pressure optical sensors. Linked to a controller system, the collected data would be treated in real time aiming to identify the location of transition and then sending a signal to the actuator system to adjust the wind surface to delay the transition location. Several measurement techniques for transition detection were developed in the past using various pressure transducers such as microphones [4], hot films [5–8], and piezoelectric [9] and Kulite sensors [10]. Usually, this type of transducer could be intrusive to the flow past the wing. In this paper, to avoid such transducer and flow interaction, optical sensors are chosen as they can be mounted right on the model surface with sealed taps.

In the present theoretical and experimental investigation, the performance of the pressure optical sensors is assessed in static and dynamic modes. Unsteady pressure signals were recorded and reduced for wind-tunnel wall interference. The measured data were confronted against pressure tap and Kulite transducers data. Flow simulations, using XFOIL code, were also performed for the same wind-tunnel flow conditions and the predicted results, obtained in terms of pressure coefficients and transition location, were compared with the measured data, for various Mach numbers, angles of attack, and Reynolds numbers. Relative errors are calculated and shown in Sec. IV.

## II. Experimental Setup Description

The wind-tunnel tests were performed at the Institute for Aerospace Research at the National Research Council Canada Uplands facilities in Ottawa. The purpose of these tests was to verify the

Received 31 August 2008; revision received 16 December 2008; accepted for publication 16 November 2008. Copyright © 2008 by Ruxandra Mihaela Botez. Published by the American Institute of Aeronautics and Astronautics, Inc., with permission. Copies of this paper may be made for personal or internal use, on condition that the copier pay the \$10.00 per-copy fee to the Copyright Clearance Center, Inc., 222 Rosewood Drive, Danvers, MA 01923; include the code 0021-8669/09 \$10.00 in correspondence with the CCC.

\*Ph.D. Student, Laboratory of Research in Active Controls, Avionics and AeroServoElasticity LARCASE, 1100 Notre-Dame West Street. Member AIAA.

†Professor, Laboratory of Research in Active Controls, Avionics and AeroServoElasticity LARCASE, 1100 Notre-Dame West Street. Member AIAA.

‡Associate Research Officer, Institute of Aeronautical Research, Montreal Road, Uplands Building U66. Member AIAA.

§Postdoctoral Fellow, Laboratory of Research in Active Controls, Avionics and AeroServoElasticity LARCASE, 1100 Notre-Dame West Street. Member AIAA.

capabilities of optical sensors to detect the pressures and flow transition on a half-wing in a wind tunnel. This wing had a NACA 4415 airfoil with a span of 4 ft (1.2 m) and a chord of 18 in. (0.4572 m), and was equipped with nine pressure taps (PT) connected to a Scanivalve ZOC<sup>TM</sup>Kulite, one Kulite (KU) sensor, and four optical sensors (OS). Their positions on the wing are shown in Fig. 1. The Kulite sensor was connected through the Precision Filter 27000. The filter provides a 6-pole butterworth function and the sampling rate was set to 1 kHz for the entire test. The Kulite has a sensitivity of 18.14 mV/psi at 5 V excitation. The Precision Filter gain was set to 100 providing a full scale voltage at 2.5 psi of 4.535 V to the electrical interface module. The optical sensors were set to provide 1 V/0.5 psi out of the analog output port which corresponds to 5 V at 2.5 psi.

The optical sensors used in this experiment are microelectromechanical systems based fiber optic pressure sensors of 2.5 mm, diameter of 10 mm, range of 5 psid, resolution less than 0.0005 psi, and precision of  $\pm 0.005$  psi.

The pressure taps and Kulite sensor were referenced to the wind-tunnel static pressure during the test runs, whereas the optical sensors were not referenced. The optical sensors were set to zero before the test was run, their indications giving a gage pressure with respect to the static pressure value of the wind off air.

The pressure information for pressure taps, Kulite sensor, and optical sensors was recorded through 18 channels; for redundancy two channels were used for each optical sensor. Optical sensors OS2, 3, and 4 were installed at the same chord position  $x/c$  as two pressure taps; PT2, OS2, and PT3 were installed at the same  $x/c = 0.3$ ; PT4, KU, and PT5 were installed at the same  $x/c = 0.4$ ; PT6, OS3, and PT7 were installed at the same  $x/c = 0.5$ ; and PT8, OS4, and PT9

were installed at the same  $x/c = 0.625$ . Only the first optical sensor was installed at different  $x/c$  as follows: PT1 was installed at  $x/c = 0.2$ , OS1 was installed at  $x/c = 0.25$ , and PT2 was installed at  $x/c = 0.3$ .

The model was installed vertically in the wind tunnel for 21 airflow cases characterized by three Mach numbers  $M = 0.1, 0.15, \text{ and } 0.2$  and seven angles of attack  $\alpha = 3, 2, 1, 0, -1, -2, \text{ and } -3$  deg. The wind-tunnel tests were conducted as follows: for each angle-of-attack  $\alpha$  setting, a “run” was recorded during which the airspeed was varied from Mach number  $M = 0.1$ , which was recorded as “point number 1,” to Mach number  $M = 0.15$ , which was recorded as “point number 2,” and finally to Mach number  $M = 0.2$ , which was recorded as “point number 3.” Figure 1 shows the positions of the sensors on the upper surface airfoil of the wing.

### III. Wind-Tunnel Data Postprocessing Details

An offset was observed between the pressures taps and the optical sensors values, as gage pressure signals were first visualized as shown in Fig. 2. It was found that three pressure taps gave wrong signals, as their tubes were pinched during installation. The pinched tube pressure signals could be identified as signals with the least oscillations, whereas they (the pinched tube signals) show the highest offsets from the theoretical calculated pressures (predicted pressure values). Figure 2 shows the time history for a pinched tube signal PT7, a correct pressure tap signal PT6, and an optical sensor signal OS3.

We observed that the offsets between the mean pressure values of OS and PT followed uniform rule variations with Mach number  $M$  and angle of attack  $\alpha$ , as shown in Fig. 3, which led to the conclusion that calibration errors of optical sensors were done. We observed that these offsets shown in Fig. 3 have the same shape as the static temperature variations during the 21 tests shown in Fig. 4. In both Figs. 3 and 4, the abscise axes showed the run numbers in chronological order from 1 to 21 (Table 1).

When the temperature recorded during these 21 runs was verified, a static temperature increase was observed when the wind was on. The first run static temperature was found below the static air temperature when the wind was off, but during the next runs, due to the air friction with the tunnel walls and screens, the static temperature increased as shown in Fig. 4. At the 19th test point, the automatic cooling system of the wind tunnel activated, causing a static temperature sudden decrease from 302 to 296.7°C.

Each optical sensor was calibrated at the beginning of the tests at the static temperature wind off  $T_0$ , which corresponds to the total air temperature. The static temperature  $T_0$  at each optical sensor position was calculated with the following equation:

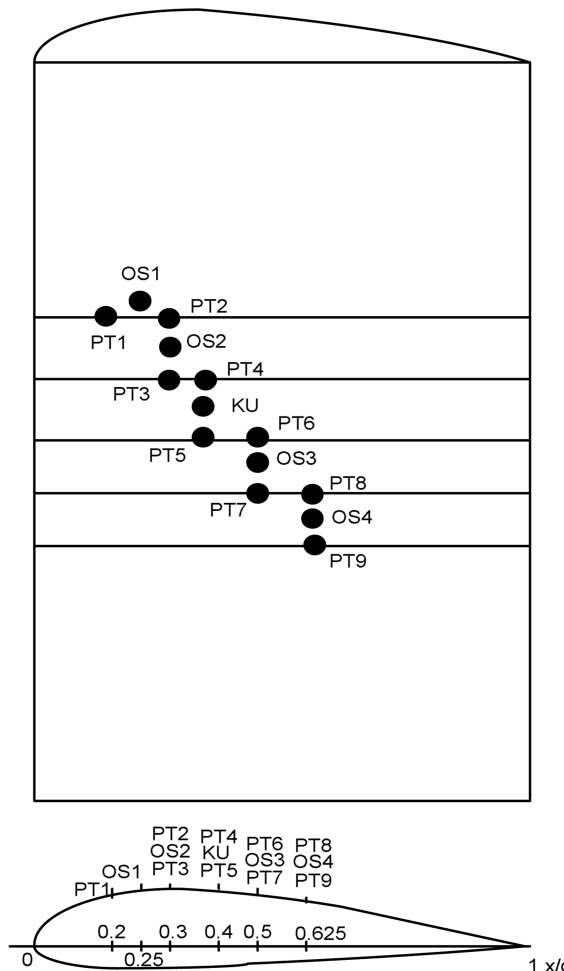


Fig. 1 Positions of the sensors on the upper surface airfoil during a wind-tunnel test.

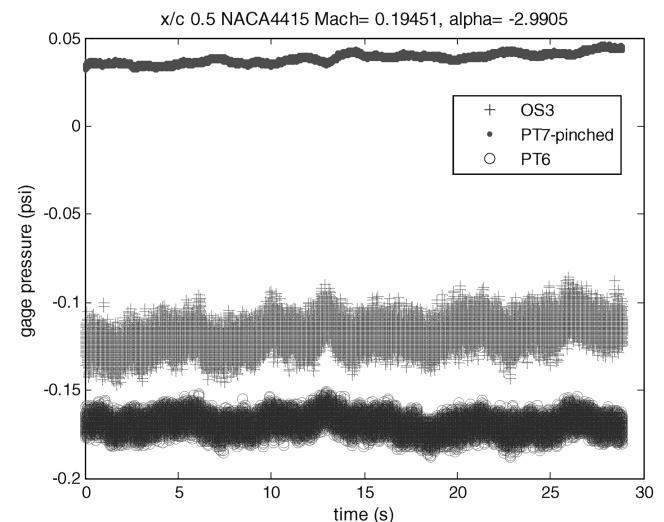


Fig. 2 Gage pressure signals recorded by optical sensors and pressure taps during 29 s.

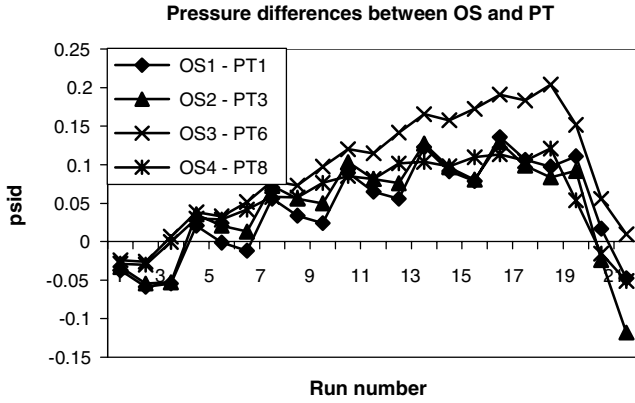


Fig. 3 Differential pressures between gage pressures measured by OS and gage pressures measured by PT.

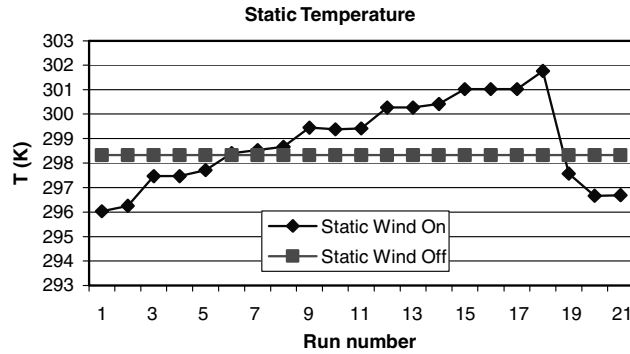


Fig. 4 Static air temperature variations during 21 runs in the wind tunnel.

$$T_0 = T_{s\infty}(1 + 0.2M_\infty^2) = T_{sOS}(1 + 0.2M_{OS}^2) \quad (1)$$

The optical sensor pressure coefficients  $C_{pOS}$  were calculated from their recorded mean pressures in the wind tunnel by use of Eq. (2). The airflow speeds  $V_{OS}$  at the location of optical sensors were calculated with Eq. (3) from their pressure coefficients. Then, the local Mach number  $M_{OS}$  was further calculated for the airflow at the location of each optical sensor from the knowledge of their correspondent airflow speeds  $V_{OS}$  by Eq. (4):

Table 1 Airflow cases dependent on angles of attack  $\alpha$ , Mach numbers  $M$ , Reynolds numbers  $Re$ , and static temperature winds on  $T_{static}$

Airflow case	Angle of attack $\alpha$ , deg	Mach no.	Reynolds no.	Static temperature wind on, K
1	0.1842	0.102	1.04e + 06	296.03
2	0.1691	0.1546	1.58e + 06	296.26
3	0.172	0.1951	1.98e + 06	297.47
4	-2.98	0.1014	1.03e + 06	297.64
5	-2.98	0.1542	1.57e + 06	297.71
6	-2.99	0.1945	1.96e + 06	298.41
7	-1.92	0.1014	1.03e + 06	298.53
8	-1.92	0.1534	1.55e + 06	298.66
9	-1.92	0.1947	1.96e + 06	299.45
10	-0.87	0.1005	1.02e + 06	299.38
11	-0.87	0.1534	1.55e + 06	299.42
12	-0.87	0.1946	1.95e + 06	300.27
13	1.242	0.1007	1.01e + 06	300.27
14	1.237	0.1534	1.54e + 06	300.42
15	1.236	0.1942	1.94e + 06	301.02
16	2.279	0.1006	1.01e + 06	301.02
17	2.275	0.1532	1.53e + 06	301.02
18	2.275	0.1937	1.93e + 06	301.77
19	3.317	0.1008	1.03e + 06	297.57
20	3.313	0.154	1.57e + 06	296.67
21	3.312	0.1958	1.99e + 06	296.69

$$C_{pOS} = \frac{\Delta p_{OS}}{Q_\infty} \quad (2)$$

$$V_{OS} = U_\infty \sqrt{1 - C_{pOS}} \quad (3)$$

$$M_{OS} = \frac{V_{OS}}{a(T_\infty)} \quad (4)$$

The optical sensor static temperature  $T_{sOS}$  was further calculated with Eq. (1), in which  $T_{s\infty}$  was the air static temperature when the wind was on. The correction was made by use of optical sensor pressure variation with temperature provided by the sensor manufacturer (Table 2) as follows:

$$\Delta p = \frac{dp}{dT} \Delta T + \Delta_r p \quad (5)$$

where  $\Delta T$  was the difference between the temperature calculated at the sensor location  $T_{sOS}$  and the temperature of its calibration from the test beginning  $T_s$ . We used the value of static temperature of 296 K (23°C) as reference temperature for sensor correction. Each optical sensor has a pressure deviation with the temperature  $\Delta p/\Delta T$  of 0.026–0.037 psi/°C and a temperature reading deviation  $\Delta_r p$  (see Table 2).

#### IV. Results Analysis

Each airflow case was simulated in Xfoil code to predict the  $C_p$  distribution and transition point position.  $N_{cr} = 7$  was used in the simulation to match the turbulence level of 0.14% measured in the wind tunnel using Mack's correlation [11]. The simulated gage pressures on the NACA 4415 airfoil calculated by use of the Xfoil code were traced versus the gage pressures measured by pressure taps PT, by optical sensors, by corrected optical sensors OS by use of Eq. (5), and by Kulite sensors KU. These types of results were traced for each airflow case from 1 to 21. An example of the plotted results is shown in Fig. 5.

The optical and Kulite sensor's gage pressures were compared versus the gage pressures measured by pressure taps for all 21 runs by use of relative error calculations. The gage pressure is defined as follows:

$$p_{gage} = p_{abs} - p_0 = \frac{\rho V_\infty^2}{2} (C_p - 1) \quad (6)$$

where  $p_0$  is the total pressure defined in Eq. (7) and  $C_p$  is defined as the pressure coefficient in Eq. (8):

$$p_0 = p_\infty + \frac{\rho V_\infty^2}{2} \quad (7)$$

$$C_p = \frac{p_{abs} - p_\infty}{\frac{\rho V_\infty^2}{2}} \quad (8)$$

Then, the gage pressure relative error is defined as follows:

$$\text{error}_{gage} = \frac{|p_{gageOS} - p_{gagePT}|}{p_{gagePT}} \quad (9)$$

Table 2 Optical sensor readings with respect to temperature and pressure variations given by the manufacturer

OS no.	Temperature deviation psi/°C	Reading deviation of mean pressure, psi
OS1	0.037	-1.11%
OS2	0.03	-0.65%
OS3	0.037	-1.02%
OS4	0.026	-0.62%

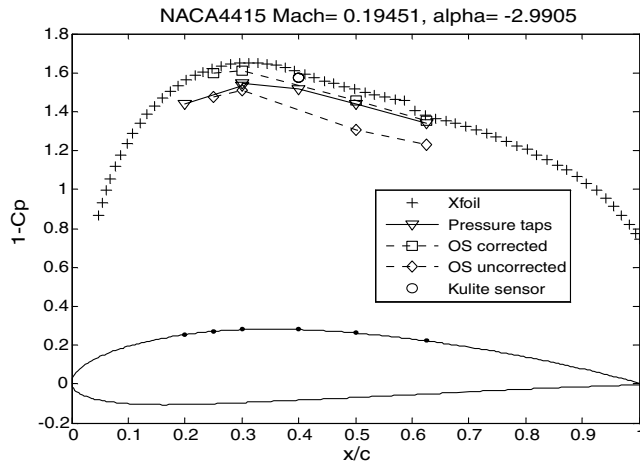


Fig. 5 Pressure coefficients distribution plotted over the wind-tunnel model airfoil's upper surface.

The relative errors for gage pressure measured by optical sensors versus the gage pressure measured by pressure taps are given in Table 3. Gage pressure of the first optical sensor cannot be compared to gage pressure for the first pressure tap as they are not at the same chord position  $x/c$ .

From Table 3, only results obtained for case 19 are the worst, which is the case when the cooling system of the wind tunnel automatically activated. These results are visualized in Fig. 6.

The relative errors for gage pressures measured by optical sensors versus the gage pressures calculated with the Xfoil computational fluid dynamics code at the same chord positions are given in Table 4.

## V. Transition Detection

From the direct visualization of signals recorded during wind-tunnel tests, it was observed that optical sensors' signals were much noisier than the pressure taps and Kulite sensors.

The turbulent waves begin to develop in the range of Tollmien–Schlichting frequency of  $\sim 1000$  Hz [9,12]. Therefore, the optical sensors acquisition unit, according to the Shannon–Nyquist theorem, should have the minimum sampling rate frequency of 2000 Hz to

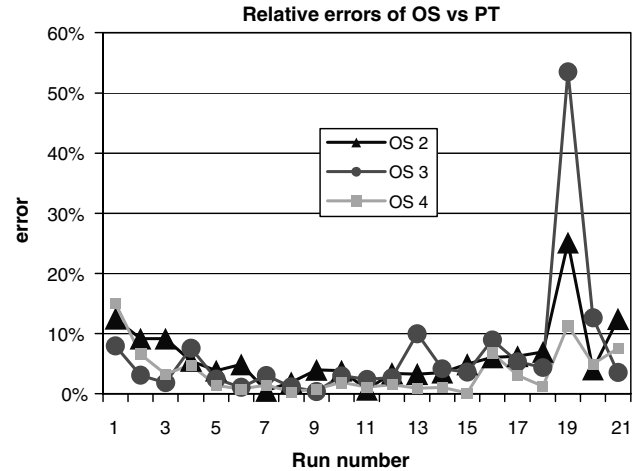


Fig. 6 Visualization of relative errors of optical sensors versus pressure taps during 21 runs in the wind tunnel.

detect the flow transition, and the optimum sampling rate should be 4000 Hz [9,13]. Because of the fact that the optical sensors acquisition unit had the sampling frequency of 1000 Hz, it was not possible to detect the airflow transition.

## VI. Conclusions

It was found that optical sensors can be used for the pressure measurements on the surface of the model, provided that each sensor has a thermocouple installed at the same position. These thermocouples should provide the optical sensor static temperatures for an accurate reading of their pressures. A new feature in this paper is the correction of the optical sensor readings using the static temperature recorded in the airflow upstream of the wind-tunnel test section.

In the absence of thermocouples, the local temperature at the position of each optical sensor was estimated as shown in the previous paragraph. By taking into account the various elements that might introduce errors, fairly accurate pressure readings were obtained.

The turbulent boundary-layer investigation demonstrated that optical sensors were found to be a good alternative to the classical

Table 3 Relative errors between OS and PT measured results for 21 airflow cases

Run no.	$\alpha$	$M$	OS2-PT2	OS3-PT6	OS4-PT8
1	0.17	0.102	12.51%	7.92%	15.03%
2	0.17	0.154	9.15%	3.06%	6.54%
3	0.17	0.195	9.13%	1.83%	3.26%
4	-2.98	0.101	5.52%	7.60%	4.81%
5	-2.98	0.154	3.82%	2.49%	1.39%
6	-2.98	0.195	4.87%	1.09%	0.79%
7	-1.92	0.101	0.51%	3.06%	1.44%
8	-1.92	0.153	1.89%	1.12%	0.31%
9	-1.92	0.195	3.98%	0.40%	0.73%
10	-0.87	0.101	3.88%	2.95%	1.87%
11	-0.87	0.153	0.69%	2.41%	1.13%
12	-0.87	0.195	3.39%	2.68%	1.53%
13	1.24	0.101	3.30%	10.00%	0.93%
14	1.24	0.153	3.53%	4.16%	1.09%
15	1.24	0.194	4.95%	3.61%	0.15%
16	2.28	0.101	6.08%	8.95%	6.78%
17	2.28	0.153	6.23%	5.27%	3.11%
18	2.28	0.194	6.93%	4.36%	1.29%
19	3.31	0.101	25.13%	53.49%	11.33%
20	3.31	0.154	4.02%	12.62%	4.91%
21	3.31	0.196	12.40%	3.52%	7.53%
Mean error of OS versus PT pressures for 21 cases			6.28%	6.79%	3.62%

Table 4 Mean error between OS measured and Xfoil calculated pressures for 21 airflow cases

Run no.	$\alpha$	$M$	OS1 vs Xfoil	OS2 vs Xfoil	OS3 vs Xfoil	OS4 vs Xfoil
1	0.17	0.102	4.53%	2.32%	2.61%	5.57%
2	0.17	0.154	7.94%	4.84%	6.82%	0.87%
3	0.17	0.195	8.37%	5.23%	5.49%	4.07%
4	-2.98	0.101	3.08%	5.13%	1.24%	1.16%
5	-2.98	0.154	1.77%	4.21%	1.96%	3.63%
6	-2.98	0.195	1.55%	2.41%	3.72%	1.98%
7	-1.92	0.101	3.13%	8.68%	1.58%	3.16%
8	-1.92	0.153	0.66%	4.79%	2.86%	2.95%
9	-1.92	0.195	1.11%	2.90%	4.99%	3.66%
10	-0.87	0.101	2.71%	14.80%	9.72%	5.16%
11	-0.87	0.153	6.48%	9.91%	10.17%	6.33%
12	-0.87	0.195	5.35%	6.52%	8.17%	6.21%
13	1.24	0.101	6.53%	16.11%	17.79%	6.60%
14	1.24	0.153	8.71%	10.40%	10.70%	5.97%
15	1.24	0.194	9.93%	9.34%	10.60%	7.10%
16	2.28	0.101	1.95%	8.46%	13.41%	1.02%
17	2.28	0.153	8.88%	9.08%	12.74%	4.66%
18	2.28	0.194	10.40%	8.75%	12.41%	6.62%
19	3.31	0.101	41.65%	35.96%	56.87%	18.18%
20	3.31	0.154	21.72%	11.98%	20.49%	3.70%
21	3.31	0.196	15.28%	4.46%	11.27%	1.02%
Mean errors for 21 cases			8.18%	8.87%	10.74%	4.74%

present technologies using Kulite sensors or piezoelectric or hot film sensors, provided the acquisition unit of the optical signal has a minimum sampling rate of 2000 Hz.

### Acknowledgments

We would like to thank the Consortium of Research in the Aerospace Industry in Quebec (CRIAQ), Thales Avionics, Bombardier Aerospace, and the National Sciences and Engineering Research Council (NSERC) for the support that made this research possible. We would also like to thank George Henri Simon for initiating the CRIAQ 7.1 project, and Philippe Molaret from Thales Avionics and Eric Laurendeau from Bombardier Aeronautics for their collaboration on this work. Thanks are due also to Teodor Lucian Grigorie for his advice during this work.

### References

- [1] Jacob, J. D., "On the Fluid Dynamics of Adaptive Airfoils," *Proceedings of 1998 ASME International Mechanical Engineering Congress and Exposition*, American Society of Mechanical Engineers, Fairfield, NJ, 15–20 Nov. 1998, pp. 1–10.
- [2] Driver, J., and Zingg, D. W., "Optimized Natural-Laminar-Flow Airfoils," *44th AIAA Aerospace Sciences Meeting and Exhibit*, AIAA, Reston, VA, 9–12 Jan. 2006, pp. 1–16; also AIAA Paper 2006-247, 2006.
- [3] Zingg, D. W., Diosady, L., and Billing, L., "Adaptive Airfoils for Drag Reduction at Transonic Speeds," *24th Applied Aerodynamics Conference*, AIAA, Reston, VA, 5–8 June 2006, pp. 1–15; also AIAA Paper 2006-3656, 2006.
- [4] Rioual, J.-L., Nelson, P. A., and Fisher, M. J., "Experiments on the Automatic Control of Boundary-Layer Transition," *Journal of Aircraft*, Vol. 31, No. 6, 1994, pp. 1416–1418.  
doi:10.2514/3.46668
- [5] Mangalam, S. M., "Real-Time Extraction of Hydrodynamic Flow Characteristics Using Surface Signature," *IEEE Journal of Oceanic Engineering*, Vol. 29, No. 3, July 2004, pp. 622–630.  
doi:10.1109/JOE.2004.833098
- [6] Krishnan, V., Sundaram, S., and Viswanath, P. R., "Transition Related Studies on Two Low-Drag Airfoils," *Current Science*, Vol. 79, No. 6, 2000, pp. 829–833.
- [7] Khalid, M., "The Use of Hot-Film Technique for Boundary Layer Studies on a 21% Thick Airfoil," *Aeronautical Note NAE-AN-45*, NRC No. 27892, Ottawa, May 1987.
- [8] Haussmann, F., and Schroder, W., "Coated Hot-Film Sensors for Transition Detection in Cruise Flight," *Journal of Aircraft*, Vol. 43, No. 2, March–April 2006, pp. 456–465.  
doi:10.2514/1.14825
- [9] Nitsche, T., Mirov, P., and Dorfler, T., "Investigations on Flow Instabilities on Airfoils by Means of Piezofoil-Arrays," *Laminar-Turbulent Transition IUTAM Symposium Toulouse, France 1989*, Springer-Verlag, Berlin/Heidelberg, 1990, pp. 129–135.
- [10] Tang, F. C., and Brown, D., "Flow Quality Measurements in the NAE 5 FT × 5 FT Blowdown Wind Tunnel Using an Instrumented 10° Cone," 53rd Semianual Meeting of the Supersonic Tunnel Association at the NASA Ames Research Center, 26–28 March 1980.
- [11] Drela, M., "Implicit Implementation of the Full en Transition Criterion," *21st Applied Aerodynamics Conference*, AIAA, Reston, VA, 23–26 June 2003, pp. 1–8; also AIAA Paper 2003-4066, 2003.
- [12] Schubauer, G., and Skramstad, H., "Laminar Boundary Layer Oscillations and Transition on a Flat Plate," NACA TR 909, 1947.
- [13] Lee, T., Petrakis, G., Kafyeke, F., and Mokhtarian, F., "Non-Intrusive Characterization of the Airfoil Boundary Layer at Low Reynolds Numbers," *Canadian Aeronautics and Space Journal*, Vol. 45, No. 1, March 1999, pp. 9–16.